Numerical and Empirical Studies on Friction Stir Welding of Yellow Brass 405-20

Syed Farhan Raza
University of Engineering and Technology
Sarmad Ali Khan
University of Engineering and Technology
Muhammad Farhan
University of Engineering and Technology
Naveed Ahmed
Al Yamamah University
Muhammad Salman Habib
University of Engineering and Technology
Ahmed M. Mehdi (a.mehdi@uq.edu.au)
The University of Queensland

Research Article

Keywords: Friction Stir Welding, Brass, Simulations, Hardness, Ultimate Tensile Strength, Thermal Distribution

Posted Date: October 18th, 2021

DOI: https://doi.org/10.21203/rs.3.rs-980005/v1

Numerical and Empirical Studies on Friction Stir Welding of Yellow Brass 405-20

Syed Farhan Raza [a], Sarmad Ali Khan [a], Muhammad Farhan [b], Naveed Ahmed [c], Muhammad Salman Habib [a], Ahmed M. Mehdi[1, d]

[a] Department of Industrial and Manufacturing Engineering, University of Engineering and Technology, G.T. Road, 54890, Lahore, Punjab, Pakistan

[b] Department of Mechanical Engineering, University of Engineering and Technology, G.T. Road, 54890, Lahore - New Campus, Punjab, Pakistan

[c] Department of Industrial Engineering, College of Engineering and Architecture, Al Yamamah University, Riyadh 11512, Saudi Arabia.

[d] The University of Queensland Diamantina Institute, Faculty of Medicine, The University of Queensland, Translational Research Institute, Brisbane, QLD, Australia

Abstract

Friction stir welding (FSW) is an eco-friendly and solid-state joining technology. Due to this reason, industries are keenly adopting this joining process in their various applications e.g., automobile, aerospace, marine, etc. Several materials have already been welded by FSW including aluminum, copper, steel, alloys of these materials, plastics, composites, and list are still going on. Few researchers have welded the brass using FSW. In this research, yellow brass 405-20 is welded with FSW for the very first time. Thermal distribution during FSW of brass was recorded via both simulations and experiments. Moreover, ultimate tensile strength was also measured numerically with its validation from its empirical counterpart. Finally, hardness was measured numerically in the form of compressive strength of welded brass, and it was also validated experimentally. Three aspects of validated simulations were never studied for brass 405-20 before and finally a good and close match was found between results from both simulations and experiments.

Keywords

Friction Stir Welding, Brass, Simulations, Hardness, Ultimate Tensile Strength, Thermal Distribution

1. Introduction

Friction stir welding is famous joining technique in industry and research laboratories due to its various advantages e.g., it is fumeless, external medium less, melt less due to its solid-state nature, no protective equipment required, etc. FSW was first used for aluminum and its alloys at the Welding Institute of the United Kingdom and patented by Wayne Thomas in 1991 [1]. Now, it has been a state-of-the-art technique that is used to weld various other materials e.g., steel, magnesium, copper, plastics, composites, and dissimilar materials [2].

To determine the effect of FSW factors, few trial experiments with different combinations of FSW factors are usually made under the guidance of the most relevant literature. Sometimes,

[1] Corresponding author.
Email Address: a.mehdi@uq.edu.au
Postal Address: 20 Parkway Street, 4112 Kuraby, Queensland, Australia
Tel/Mob. No. +61734436947

trial experiments seem essential in the absence of background knowledge as the research study is never conducted before. Numerical studies play an important role in minimizing the cost and time required for trial experiments. Therefore, thermal simulations may be performed towards evaluating the suitability of weld factors which may lead to very few trial experiments to validate the evaluation of weld factors' appropriateness [3].

M Song and R Kovacevic [4] conducted a thermal study on FSW involving three dimensional (3D) transient thermal model using finite difference method. Heat generation was calculated by introducing a moving coordinate methodology. Non-uniform grid of mesh was utilized in this study to register temperature distribution easily. Numerical results were validated by the empirical data of FSW with good agreement between these results. Although authors strived their best with a numerical study, there is a dire need to perform a 3D transient thermal study with finite element analysis (FEA) leading to develop uniform mesh density. This thermal and numerical study to be conducted will further be used for determining the joint strength. Moreover, authors have conducted this study for aluminum and tool steel. Therefore, a research gap of numerical study for brass material, exists which should be filled up.

P. Biswas and N. R. Mandal [5] have developed another thermal analysis focusing mainly on the effect of the tool geometry using aluminum alloy. Effect of various tool geometries were used in this research to determine their effect on the thermal history numerically. Numerical results were found to be agreed well with those of empirical validating the various assumptions for the thermal study. Although authors have put forward another approach for thermal simulations, these are lacking various aspects of FSW to improve the inclusiveness of this study e.g., standardized joint design, effect of combination of other FSW parameters on thermal history, aluminum was again used instead of other materials, etc.

H. Zhang et al. [6] performed a thermal study in which they have managed to change the material to be welded by FSW. Finally, they used magnesium alloy AZ31 as a good applicant for FSW. This study revolves around the investigation of thermal distribution in the preheating period of FSW of AZ31 seeking appropriate preheating weld parameters. Although authors have somehow managed to numerically study the FSW of AZ31, specimen design was not standardized, magnesium alloy is based on aluminum, and measurement of temperature was accomplished using conventional k-type thermocouples.

S. Bag et al. [7] presented an idea of performing thermal analysis numerically as well as experimentally with aluminum alloys. In their study, heat input was supplied in the form of symmetric heat flux at the mating line of flat tool shoulder surface, tool pin side, and bottom surfaces. Effect of transverse tool speed was neglected. Although numerical and empirical results was agreeing with each other, aluminum was again used which should be replaced with any other novel material like brass. In a similar study on aluminum alloy, A. R. S. Essa et al. [8] found the numerical effect of eccentric cylindrical pin on the heat development during FSW. The thermal simulation was in good agreement with that of experimental, the same approach may be used for brass to see whether there still exists a very good agreement between numerical and empirical results.

H. A. Derazkola et al. [9] developed a new numerical approach based on computational fluid dynamics (CFD) to comprehend the mixing flow of materials during FSW. They strived to establish a link between the mixing of materials and bonding of materials before and after FSW respectively. Although authors have provided the research community with a novel idea of applying CFD on FSW of Al-Mg-Si alloy T-Joints, numerical study based on CFD was not validated with empirical methods. Moreover, the flow of material like a fluid is not possible, since melting of solid materials never happened during FSW which is a solid-state welding technique.

M. B. Durdanovic et al. [10] established a better way of understanding the FSW by dividing it into five growing and gradual stages with the assumption that tool is perpetually rotating during these stages. These five stages include plunging into specimens, primary dwelling, traversing/translating in a straight line, secondary dwelling, and pulling out of welded specimens. Authors have also developed a mathematical model to calculate the heat generated. Although authors have made an excellent effort to present comprehensive understanding of FSW, the mathematical model is having few inaccuracies that is why, theoretical results did not agree with experimental results.

Brass is an alloy of copper and zinc. Brass properties are determined from the careful configuration of percent copper in percent zinc. It is widely used as engineering and industrial material due to its various striking properties such as high strength, high corrosion resistance, high electrical and thermal conductivity. Brass may easily be formed when processing and it is apparently nice looking before and after processing. Brass provides a lot of difficulties when its subjected to fusion welding, since melting of brass usually involves evaporation of zinc. Hence novel joining process should be employed which don't excite the melting of brass and brass remains in its solid-state during and after welding. Friction stir welding (FSW) may be used to weld brass keeping it view that brass must not be melted. C. Meran [11] welded the brass (CW508L) which is CuZn30. Author has validated that melting of this grade of brass never observed leading preserving excelling joint properties in the presence of zinc. On the other hand, F. Hugger et al. [12] did the laser beam welding of brass and observed a huge evaporation of zinc, since melting of brass occurs during laser welding. Although the joining of brass via laser welding is novel, the properties of joined brass are greatly compromised due to the evaporation of zinc as weld interface temperature goes beyond 1200 ^{o}C justifying the viability of FSW for brass.
Few researchers have also worked on FSEW of few grades of brass which were more empirical in nature. These studies may establish a strong foundation for trial experiments along with the results from numerical studies when novel brass materials are intended to be welded by FSW.

For instance, G. Cam et al. [13] joined via FSW the two different alloys of brass separately. These alloys of brass are known as 70/30 and 90/10. Authors have found using optical microscope that no porosity exists when welding these brass alloys distinctly. This proves that there is no evidence of evaporation of zinc during welding of brass alloys. Therefore, it has been reconfirmed. Although researchers have welded brass specimens, they did address the thermal distribution at HAZ.

T. Murakami et al. [14] worked on the microstructural changes while joining brass with FSW. At HAZ, two phases were identified namely alpha and beta phases. Alpha phase was named to be the bright phase where beta phase was identified as dark phase. At a particular weld configuration, beta phase was declared to be negligible i.e., 17 – 20% as compared to the base brass where degree of this phase was present as 16%. What is the % for alpha phase at HAZ? It was concluded that evaporation of zinc was not there even in a single case of FSW, since FSW is a solid-state welding process. It was also concluded that alpha grain size decreases with decreasing the heat input. Maximum tensile strength of 550 MPa was reported by the authors which was 144% of base metal 60/40 brass. This weld strength decreases due to the defect's formation at the HAZ due to non-recrystallization of alpha phase of brass. A. Heidarzadeh et. al. [15] reported the defects formation in their study on microstructure of 63/37 brass. They employed optical microscope, scanning electron microscope (SEM), and scanning transmission electron microscope (STEM) to study the microstructure of brass under investigation. It was revealed that the alpha grains resulted in dynamic recrystallization (DR) after FSW into finer grains. However, beta phase split between the alpha grains without DR.

From the literature review, it is quite evident that very few researchers have currently focused on welding brass via FSW. Researchers have made their way to FSW using various materials and process parameters. They did substantial numerical and empirical studies. Many numerical studies were experimentally validated with materials other than brass. Most of the researcher used non-standardized samples too. Temperature distributions during welding and their predictions through numerical studies are extremely important, since these give both excellent indications of the effect of FSW weld factors on the thermal changes and assurance of temperature reach i.e., it must remain below the melting point of material under considerations. Researcher validated temperatures via k-type thermocouples with tensile strength and hardness were never studied in terms of their validations in the literature which are also caused by thermal changes during FSW. In many engineering applications such as structures, bridges, joined structures, etc., predictions of strength and hardness are also important. In other words, numerical studies were also completed for strengths and hardnesses with their proper validations. In fact, these numerical and empirical investigations pertinent to friction stir welding of brass 405-20 were never studied before at first. And numerical studies with their validations are being performed the very first time for temperature distributions, joint strength, and hardness. Hence it was required to perform numerical studies for FSW of brass with their proper validation for thermal distribution at HAZ using thermal imager that is more reliable than k-type thermocouples, tensile strength, and hardness.

2. Materials and Methods

Material and methods for Friction stir welding (FSW) process can be divided in to two categories to make it more eloquent. One is relevant to simulation work known as numerical FSW and second is relevant to experimental investigation known as empirical FSW. These two categories are further equally divided into three subcategories named as follows:

i. Preprocessing
ii. Processing

iii. Postprocessing

2.1. Numerical FSW

In this category of materials and methods, simulation work completed and investigated is presented regarding FSW of brass with following subcategories:

2.1.1. Preprocessing

In this step of numerical study, two finite element analyses (FEAs) were performed namely transient thermal and static structural in Ansys Workbench 19.2. Moreover, later finite element analysis (FEA_B) i.e., static structural was coupled to the first FEA (FEA_A) i.e., transient thermal. In other words, results from FEA_A were input to the FEA_B. Additionally, the time dependent load in the form of heat flux, as calculated from Eq. 2 [16], was applied at the joint interface by dividing it into time steps which are further based on the combination of factors' levels from each DOE from 1 to 9. FEA_A was used to find the numerical temperatures at the joint interface whereas FEA_B was utilized to determine the numerical strengths and numerical hardnesses at the joint interface.

Geometric modeling was conducted in SolidWorks software based on the ASTM standard (E8/E8M-13a), as shown in Fig 1. The geometry was imported to Ansys Workbench software. Brass material with its chemical composition, mechanical and thermal properties were assigned to the imported geometric model. These properties are shown in Table 1, 2, & 3.

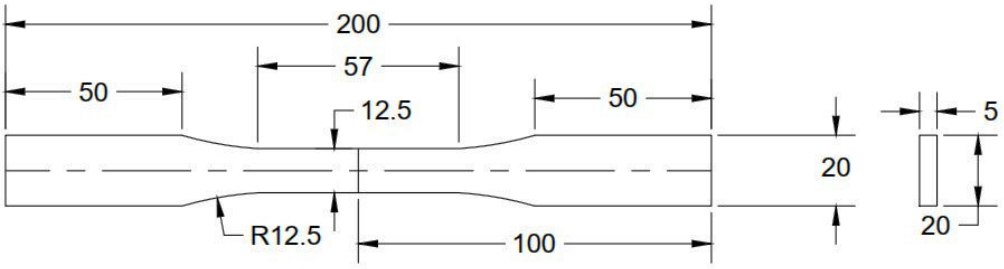

Fig. 1 ASTM Standard (E8/E8M-13a) for Weld Specimen Design

Table 1 Chemical Composition of Brass

Material	Cu	Zn	Pb	Sn
	Percentage (%)			
Brass 405-20	63.0	34.7	1.0	1.0

Table 2 Mechanical Properties of Brass

Material	UTS	Yield Strength	Hardness	Elongation (%)

	(MPa)	(MPa)	(HR-15N)	
Brass 405-20	275	250	82 avg.	15

Table 3 Thermal Properties of Brass

Material	Specific Heat (C)	Thermal Conductivity (K)	Density (ρ)	Emissivity (ε)	Melting Point (Tm)
	J/kg ^{o}C	W/m ^{o}C	Kg/m3	(600^{o}C)	^{o}C
Brass 405-20	380	119	8800	0.61	940

Contact status was defined as bonded contact in the connections definitions of preprocessing phase of Ansys.

Meshing of the geometry was accomplished after the geometry has been assigned with brass material properties mentioned in Table 1, 2 & 3. Moreover, mesh verification was completed with low, medium, and high quality of meshing. Maximum temperature found for these three qualities of meshing was almost similar. Hence mesh quality was selected as medium levels.

Eq. 1 [17] is the governing differential equation for calculating temperature numerically.

$$k\,\partial^2T/\partial x^2 + k\,\partial^2T/\partial y^2 + k\,\partial^2T/\partial z^2 + Q - \rho c\partial T/\partial t = 0 \qquad (1)$$

Where,

T = Temperature, ^{o}C (to be determined by solving Eq. 1)

K = Isotropic Thermal Conductivity of PP, W/m. ^{o}C

ρ = Density of PP, Kg/m^3

c = Specific Heat Capacity of PP, J/Kg. ^{o}C

Q = Volumetric Heat Generation Rate, W/m3. ^{o}C

Volumetric heat generation rate (Q) was given as an input heat flux at the joint interface in FEA simulation to predict the temperature at HAZ. Average power generation (q) during friction stir welding can be calculated by Eq. 2 and heat flus per unit area (Q) was calculated by Eq. 4 [16].

$$q = 2\pi * k * \omega * Rs^3/3 \qquad (2)$$

Where,

k = yield stress of brass (MPa)

ω = Rotational Speed (rad/s)

R_S = Shoulder Radius

$$Q = \frac{3 * q * Rs}{Rs^3 - Rp^3} \qquad (3)$$

Where,

q = Eq. 2

R_P = Pin Radius

Moreover, when putting q in Eq. 3, we obtain a relationship for heat flux per unit area that is shown in Eq. 4.

$$Q = \frac{k * \omega * Rs^4}{Rs^3 - Rp^3} \qquad (4)$$

Since Eq. 4 considers only the heat flux for its conduction at the solid interface of FSW joint areas, heat losses due to convection from the solid areas into the environment or air, were calculated using fundamental equation of convection heat flow, as shown in Eq. 5.

$$Q_{convection} = h * (Ts - Ta) \qquad (5)$$

Where,

h = film coefficient

Ts = Surface Temperature at the weld interface

Ta = Air/Ambient Temperature

Moreover, the surface temperature at the weld interface, was measured using transient thermal analysis and validated with the utilization of the thermal imager supplied by testo company, as shown in Fig. 2. And film coefficient (h) was calculated then by putting Q from Eq. 4 equal to $Q_{convection}$ from Eq. 5.

Fig. 2 Thermal Imager

The preprocessing details of first FEA i.e. FEA_A finishes here. And all the three steps are being explained for second FEA i.e. FEA_B. Temperature distribution at the joint interface was aimed to be found resulting from heat estimates for FSW. The temperature distribution's results were then coupled to static structural analysis where the thermal results were imported to the processing setup of static structural analysis, as can be seen in Fig. 3. The geometry, meshing, and connections were kept the same for both FEA_A and FEA_B. This FEA_B was performed to find the stresses developed at the joint interface due to temperature variations. The fundamental mathematical expression for these stresses due to thermal loads is mentioned in Eq. 6.

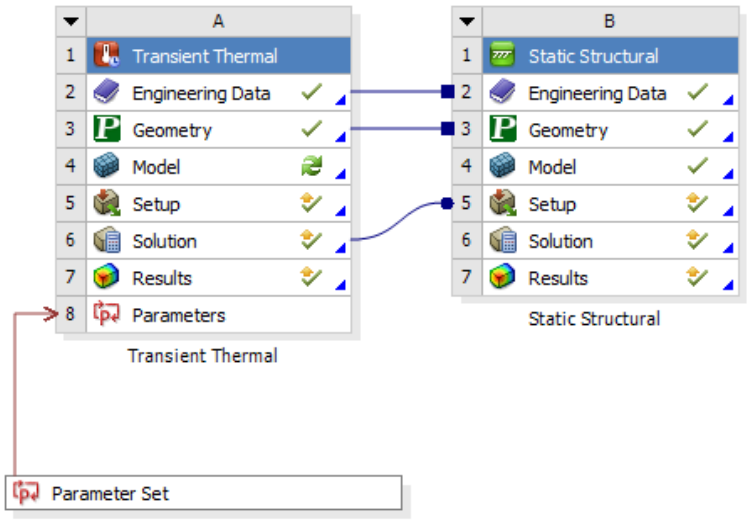

Fig. 3 Coupling Thermal Transient Analysis (FEA_A) with Static Structural Analysis (FEA_B)

$$\delta_T = \alpha * L * \Delta T \qquad (6)$$

Where,

δ_T = Change in length due to the temperature variations (mm)

α = Coefficient of thermal expansion ($/^oC$)

L = Original length (mm)

ΔT = Change in Temperature (^oC)

$$\varepsilon_T = \alpha * \Delta T \qquad (7)$$

Where,

ε_T = Thermal Strains

$$\sigma_T = E^* \varepsilon_T \qquad (8)$$

Where,

σ_T = Thermal Stresses

E = Young's Modulus

2.1.2. Processing

This phase of simulation is also called as the solution of the steps which are executed after the preprocessing phase.

In this phase of simulations, initial temperature was assigned to be equal to room/ambient temperature for all the nodes and elements.

$Q_{convection}$ calculated previously was subtracted from the heat generated from Eq. 4. The final heat calculated was given as heat flux load at the weld interface area in the form of time steps. Total number of steps and step end time were defined for the transient thermal analysis. These time steps were again based on the weld factors' levels for each DOE. Convection heat transfer was activated with the definition of film coefficient and room temperature. Therefore, processing requirements were completed at this stage. After this, the defined thermal transient system was solved under the influence of geometrical, boundary, and loading conditions.

Additionally, the geometry of ASTM specimens was fixed at its boundaries to restrict it to remain stationary during FSW, as shown in Fig. 4, for fixture. Thermal outputs from FEA_A were imported from FEA_A to FEA_B to fully setup the FEA_B. The FEA_B was now solved for finding numerically the weld strength and hardness of brass.

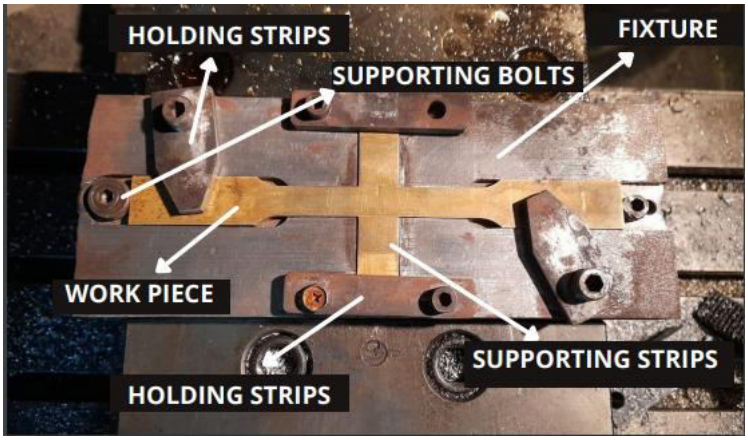

Fig. 4 Fixture holding the Specimen for FSW

2.1.3. Postprocessing

Maximum temperature was then found numerically for empirical validation from FEA_A, as shown in Fig. 5. Shear and compressive strengths were also measured numerically from FEA_B

where shear strength accounts for weld strength whereas the compressive strength represents the hardness of FSW weld, as shown in Fig. 6 and 7 respectively.

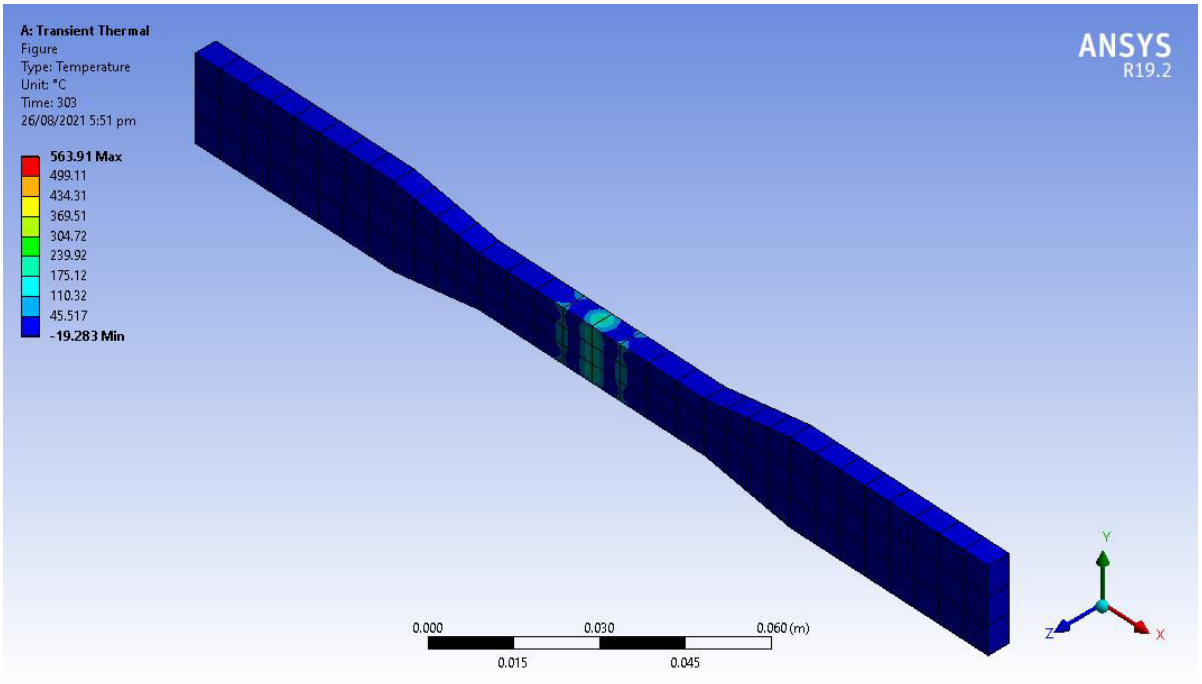

Fig. 5 Numerical results showing maximum and minimum temperatures

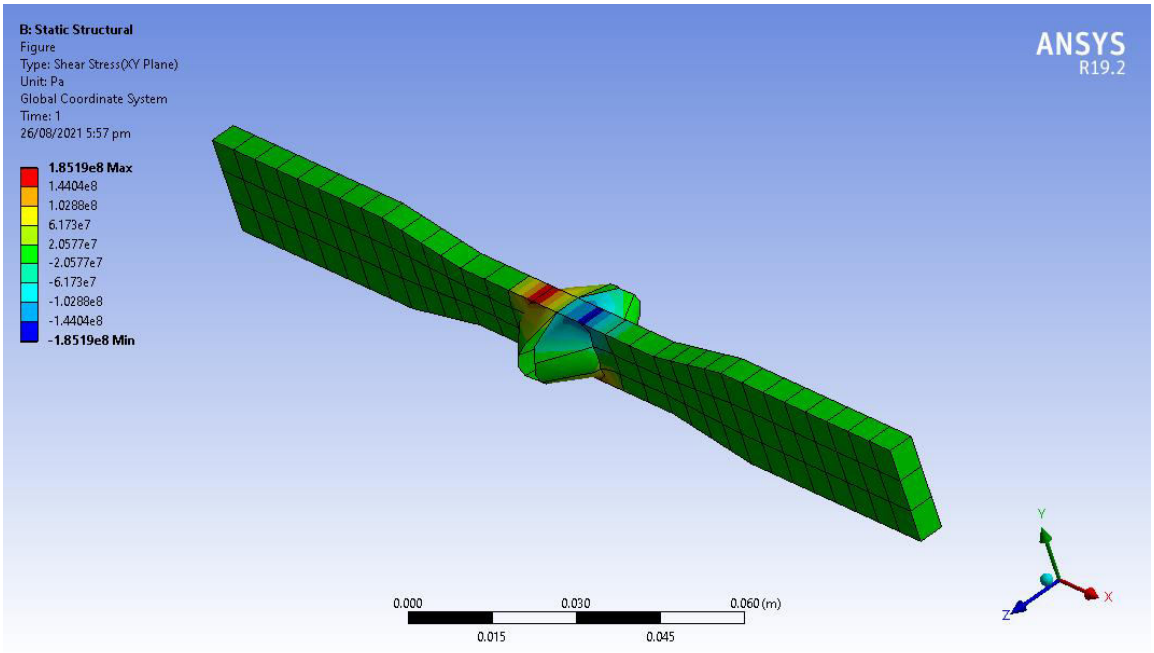

Fig. 6 Numerical results showing maximum and minimum shear strengths

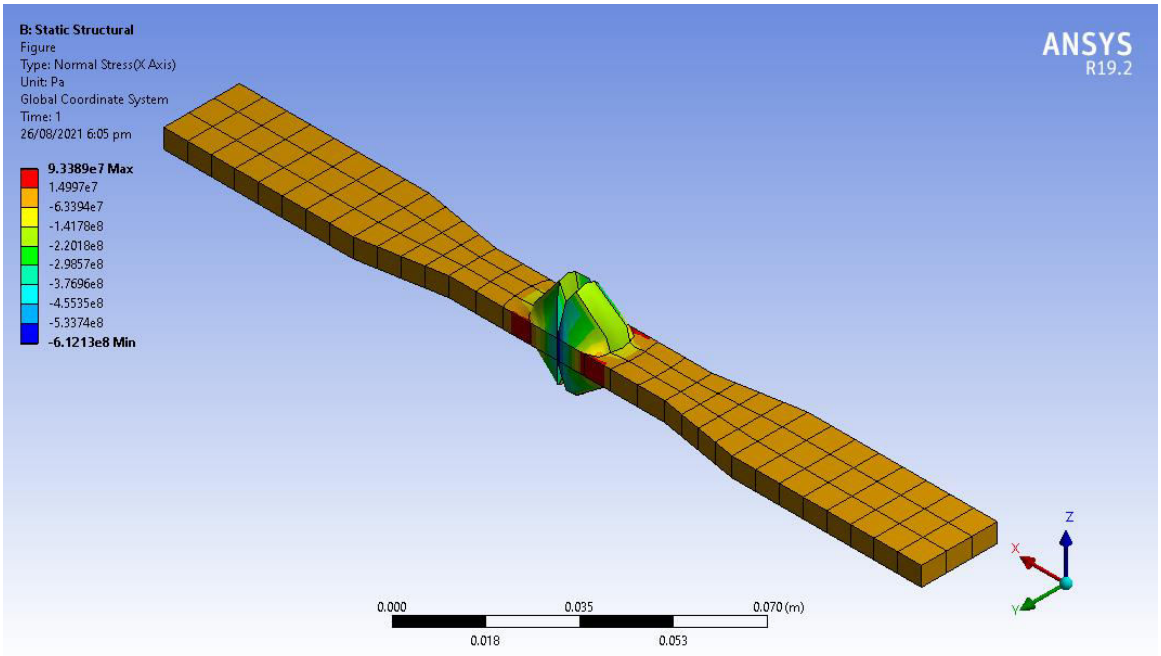

Fig. 7 Numerical results showing maximum and minimum compressive strengths/hardnesses

2.2. Empirical FSW

In this category of materials and method, a detailed experimental investigation is elaborated considering FSW of brass.

2.2.1. Preprocessing

Yellow brass 405-20 alloy of coper 63%, Zinc 34.7% and little trace in percentage of lead and tin. Specimens were manufactured in two halves according to ASTM standard E8/E8M-13a, as shown in Fig. 8. Wire electric discharge machining (EDM) were used to fabricate the samples. This alloy has the good corrosion. Filing and emery tapes were used to prepare the fabricated samples before welding.

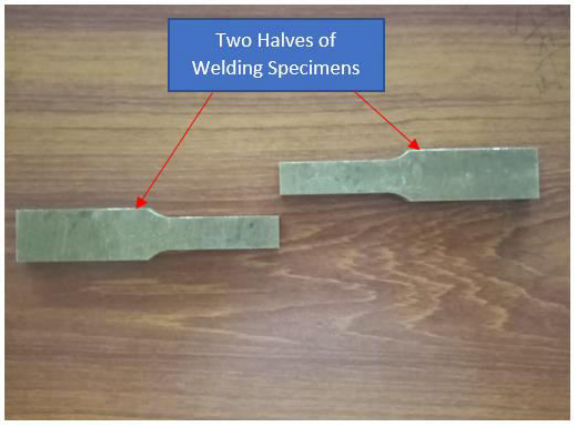

Fig. 8 Manufactured Specimens as per ASTM Standard E8/E8M-13a in two halves

Molybdenum high speed tool steels (M2 HSS) was used as tool material. M2 HSS includes

5 to 9.5 percent of molybdenum, about 4 percent chromium, 1.5 to 6.5 percent tungsten, and smaller amounts of vanadium. This tool steel is almost similar in properties to those of the H20 to H26 steels with an advantage of lower initial cost. Among those properties, this steel has the increased resistance to the thermal fatigue i.e. resistance to high temperature softening over a certain period of time.

M2 HSS was purchased in the form of cylinder rods. These rods were then turned on a conventional lathe machine with operations cutting off, facing, and turning to generate the shoulder diameter and pin diameter, as shown in Fig. 9 and 10.

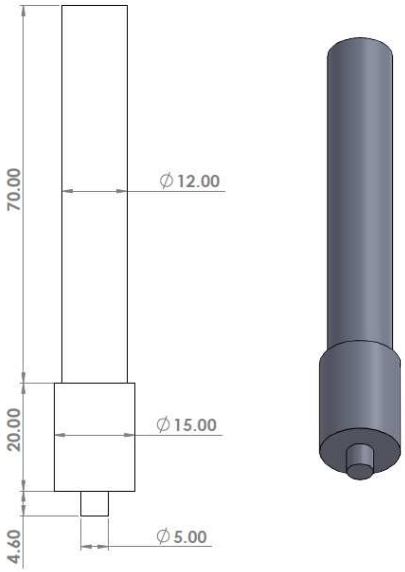

Fig. 9 FSW Tools Geometry

Fig. 10 Physical illustration of FSW Tool

A fixture was also designed and manufacturing on conventional machining center to hold the specimens so that specimens will not be allowed to move in x, y, and z directions, as shown in Fig. 4.

2.2.2. Processing

FSW was accomplished on a CNC machining center. A general FSW process is shown in Fig. 11 and 12. CNC program was written with spindle speed function (S) to account for rotational speed of FSW tool. And Feed function (F) was also specified in the CNC program for traverse speed of FSW tool. Penetration depth of FSW tool was also mentioned in the program by specifying its value in z-axis. In the same way, nine experiments were conducted with amendments in values of S & F of CNC program as per the design of experiments (DOE) based on full factorial method and factors' levels, shown in Tables 5 and 4 respectively.

Moreover, a thermal imager supplied by testo with model number 868 was also used while welding brass specimens to measure the temperature at various locations of weld line, as shown in Fig. 13. This model of imager was excellent in measuring not only the maximum temperature during FSW but also the numerous values of temperatures at any location heat affected zone (HAZ). Since researchers use k-type of thermocouple for measuring the temperature at one point of weld zone which is not only time-consuming activity but also it does not provide an opportunity to measure the joint strength and hardness due to the presence of thermocouple at HAZ, thermal image seems competent in resolving the time and effort issues during welding. Moreover, testo IRSoft software version 4.7 was used for image processing leading to measure the temperatures at multiple locations of HAZ, as shown in Fig 13 for DOE 4. In this image, there were four interfaces, top left interface shows the multiple locations of hot spot (HS) and cold spot (CS) which are the maximum and minimum temperature respectively during welding. Top right shows the temperature scale or maximum and minimum values of scale in which temperature can be measured. Bottom left interface shows the values of CS and HS. Bottom right shows the actual welding scenario schematic. Various HS can be measured along with CS using thermal imager simply through mouse clicks at different locations of top left window, the recorded HS was the maximum possible value of HS at the HAZ obtained from FSW.

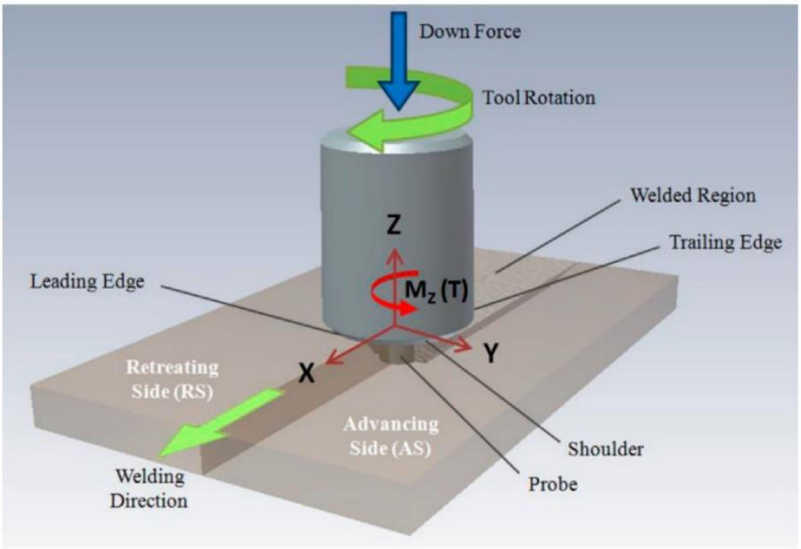

Fig. 11 Friction Stir Welding [18]

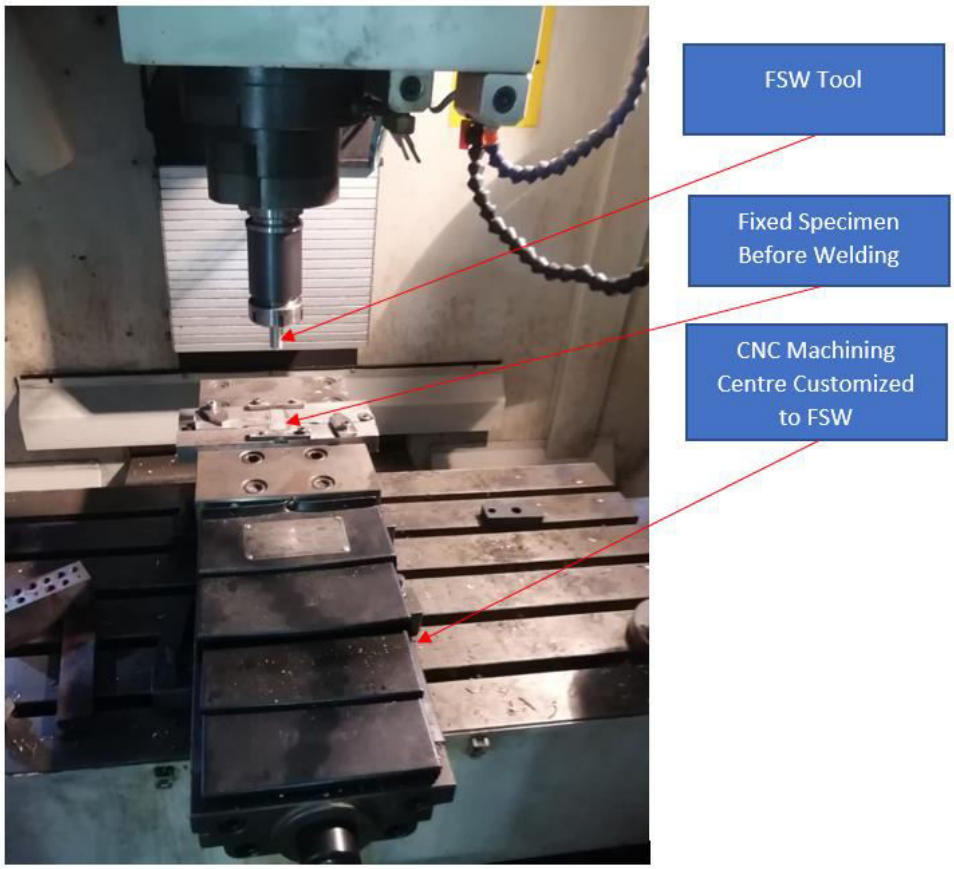

Fig. 12 Customized FSW using CNC Machining Centre

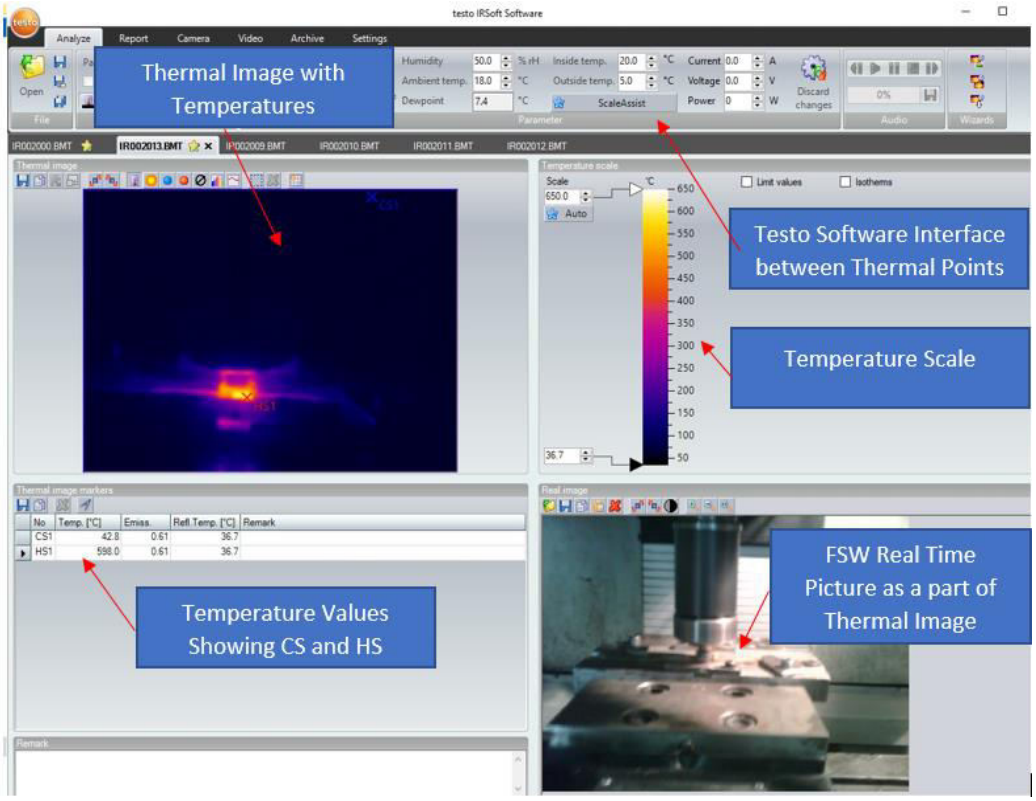

Fig. 13 An example of Thermal Image from Testo 868 Imager

Table 4 Factors' Levels for FSW of Brass

Weld Factors	Level 1	Level 2	Level 3
Rotational/Spindle Speed (rpm)	1600	1450	1300
Traverse/Welding Speed (mm/min)	60	50	40

Table 5 L-9 DOE based on Full Factorial Method

Sr. No	Rotational Speed	Traverse Speed	Revolutionary Pitch
	(Revolution per min)	(mm/min)	(Revolution per mm)
1	1600	60	26.67
2	1600	50	32.00
3	1600	40	40.00
4	1450	60	24.17
5	1450	50	29.00

Sr. No	Rotational Speed	Traverse Speed	Revolutionary Pitch
	(Revolution per min)	(mm/min)	(Revolution per mm)
6	1450	40	36.25
7	1300	60	21.67
8	1300	50	26.00
9	1300	40	32.50

2.2.3. Postprocessing

After getting the specimens welded, specimens were tested for their joint strength and hardness. Joint strength was tested using a tensometer with a crosshead speed of 1mm/min, as shown in Fig. 14. Supporting strip were also used to support the joint location for effective welding. In other words, tool enters the supporting strips on one side, transverses while rotating along the weld line of specimens, and exits again from the supporting side on the other side, as shown in Fig. 15 and 16. A broken FSW sample is also shown in Fig. 17. Side strips welded with the specimens were cut using an electric saw, as shown in Fig. 18. A sample cut by electric saw is shown in Fig. 19. Hardness was tested on the Rockwell hardness testing machine on various points, shown in the Fig. 20. Average value of hardness value was then measured. Three samples were tested for weld strength of FSW of brass. And hardness values are also the average of two values at the HAZ, as shown in Fig. 15.

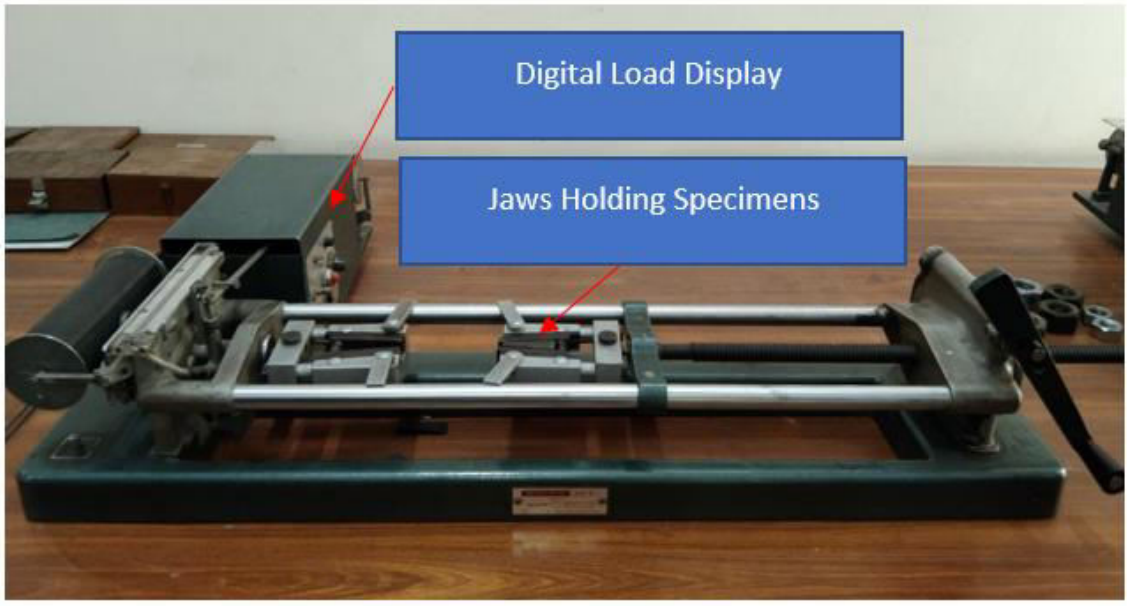

Fig. 14 Hounsfield Tensometer for measuring Friction Stir Weld Strength (FSWS)

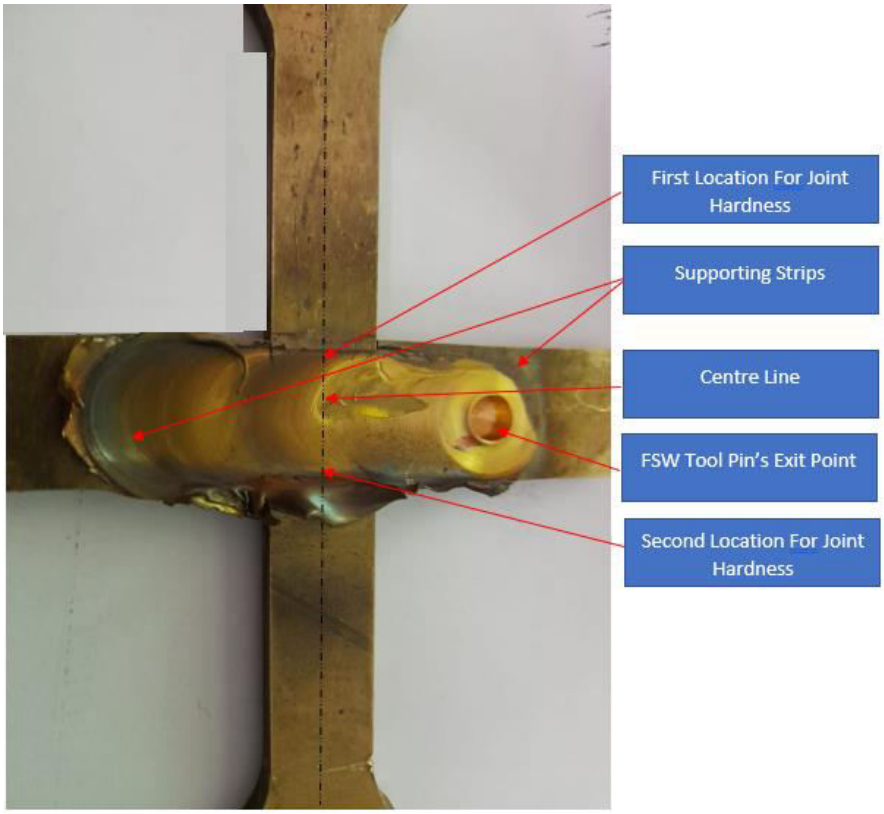

Fig. 15 A Friction Stir Weld

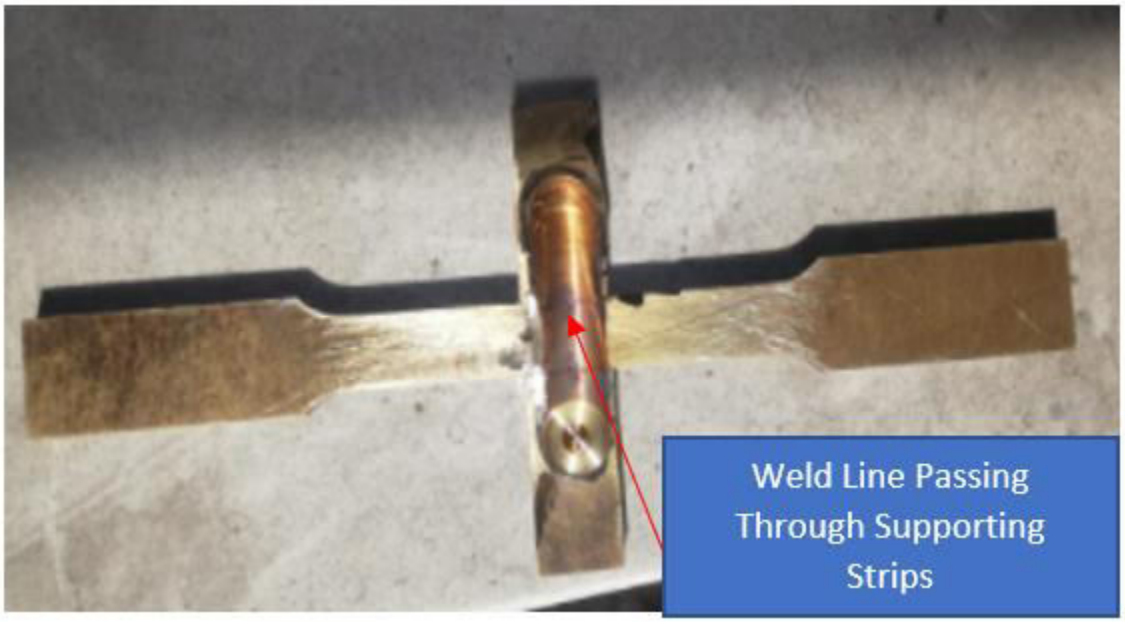

Fig. 16 FSW Sample Just After Welding

Fig. 17 A broken FSW Sample

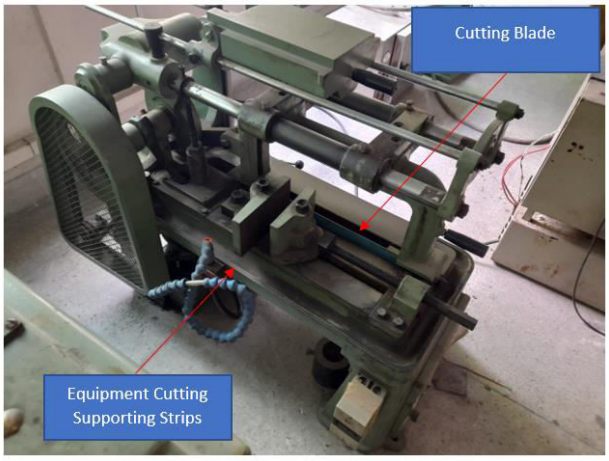

Fig. 18 Electric Saw Equipment for cutting sides of testing strips

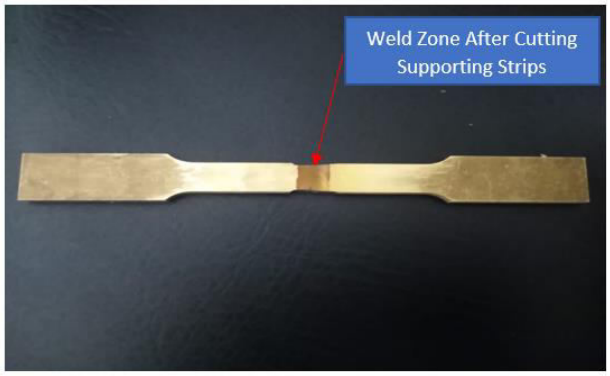

Fig. 19 A sample Cut by Electric Saw Equipment

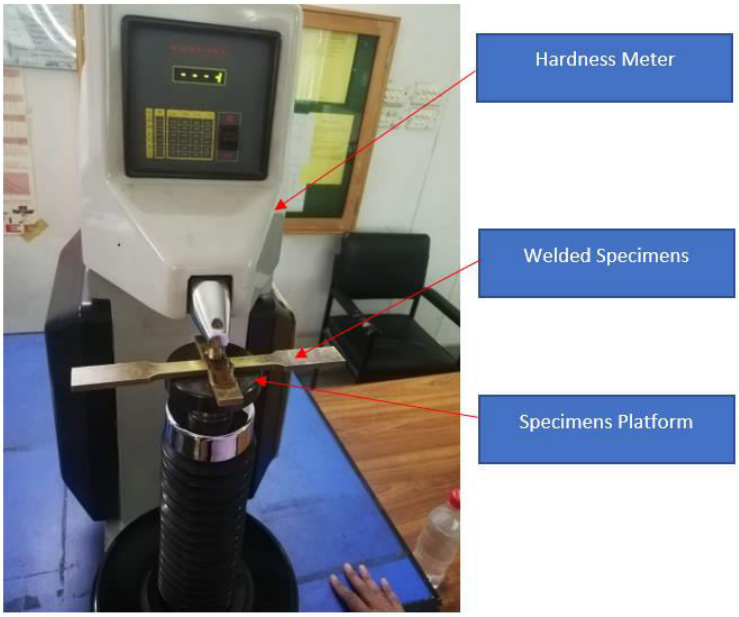

Fig. 20 Rockwell Hardness Tester

3. Results and Discussion

Results obtained from both numerical and empirical investigations, show that there exists an overall good agreement between them, as shown in Fig. 21, 22, & 23. Except there were few discrepancies in both for joint strength and few mismatches for hardness. Moreover, compressive strength was measured numerically which was validated by Rockwell hardness measurements for hardness. Comparability of hardness and compressive strength was justified by literature [19] leading to good agreement in them, as illustrated in Fig. 23.

A likely reason that compressive strength from simulations and hardness from experimental work, are minimally different from each other, is the hardness appears to be three times of strength[19]. In other words, these two are not exactly equal. However, little discrepancies between compressive strength and hardness show this work is a good effort towards equalizing them. Moreover, the mismatch only occurs for DOE4 and DOE5. In other words, hardness also shows a good agreement between compressive strength and hardness for all the experiments except DOE4 and DOE5. Hence future work will consist of considering the hardness mismatch to bring it to a good agreement.

Fig. 21, 22, & 23 show the numerical results for temperature distributions, joint strength, and hardness respectively. And Fig. 19 show that experimental FSW weld just after welding and just before shear testing in tensile fashion after removing the supporting strips using an electric power hacksaw, as shown in Fig. 18.

Moreover, the maximum temperature and joint strength was found to be the highest for DOE4 implying 1450 rpm and 60 mm/min with revolutionary pitch to be equal to 24.17 revolutions per mm, as shown in Table 5. Revolutionary pitch can be defined as a ratio of rpm and mm/min. As a result, it can be deduced that if revolutionary pitch is kept smaller then FSW weld with the maximum joint strength may be achieved. Hence it can be experimentally and numerically said that these weld factors' levels may be declared as the optimal factors' levels.

However, the hardness was found to be the lowest for DOE4 which, at first glance, negates the statement of optimal factors' levels for DOE4. In fact, this needs to be discussed in detail supporting the DOE4 as an optimal set of weld factors' levels. The lowest empirical value of hardness existing at DOE4 is 73 HR.

Highest hardness value is not appreciated, since it increases the brittleness of joint. While welding brass, copper and zinc may form intermetallic compound at the HAZ which are generally brittle in nature. Therefore, low hardness is usually desired which is amazingly found for DOE4. This validates the optimal set of weld factors at DOE4 for thermal distribution, joint strength, and hardness.

Temperature distribution indicates that maximum temperature achieved experimentally during FSW of brass, was 598 ^{o}C for DOE4. The maximum temperature was lower that the melting point of brass i.e. 940 ^{o}C. This indicates that FSW of brass was accomplished in its true spirit in terms its basic theme i.e. solid state welding technique. Moreover, evaporation of zinc will never

be observed at 598 ^{o}C requiring melting of brass. Therefore, porosity at the HAZ owing to zinc evaporation was never found even in the single experiment, as shown in Figs. 15, 16, 17, & 19.

Maximum joint strength was empirically found to be 212 MPa for DOE4 which is 77.1% of the ultimate tensile strength (UTS). The welding efficiency of joint in terms of approaching the base metal (UTS) is satisfactory that is more than 75%. This efficiency may further be improved in future considering various other weld factors e.g. tilt angle of tool, changes in the shape of pin, and changing the levels of weld factors which were currently used in this research.

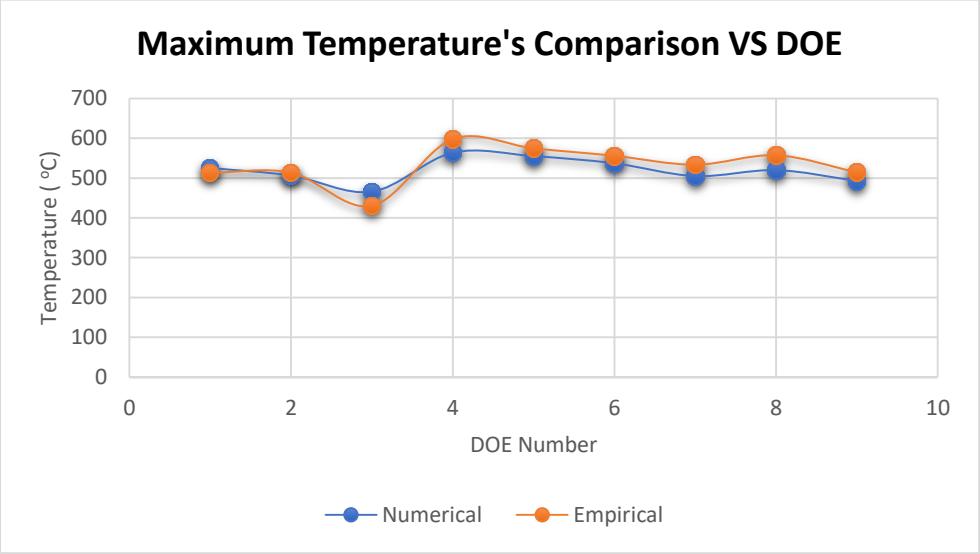

Fig. 21 Empirical validation of numerical results for maximum temperature

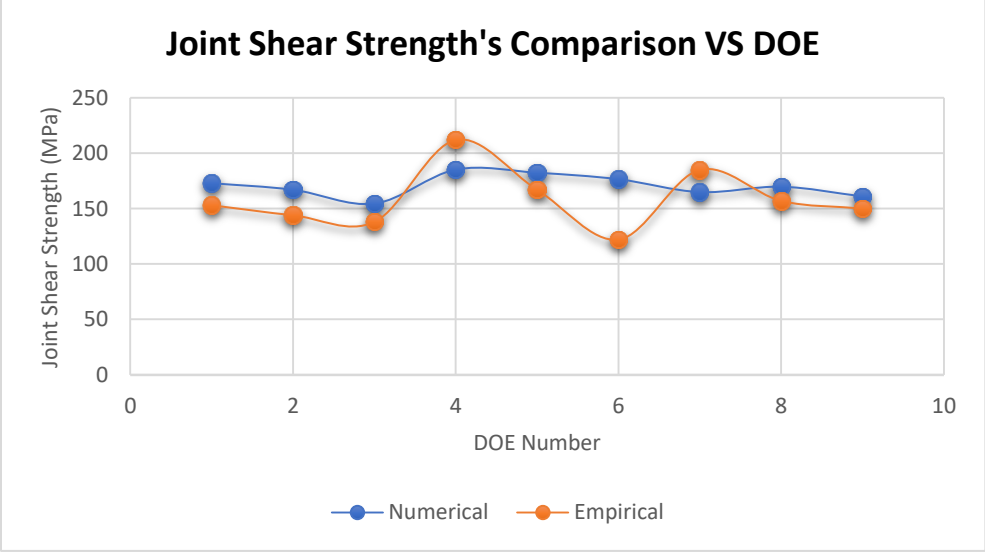

Fig. 22 Comparison of empirical and numerical weld strength

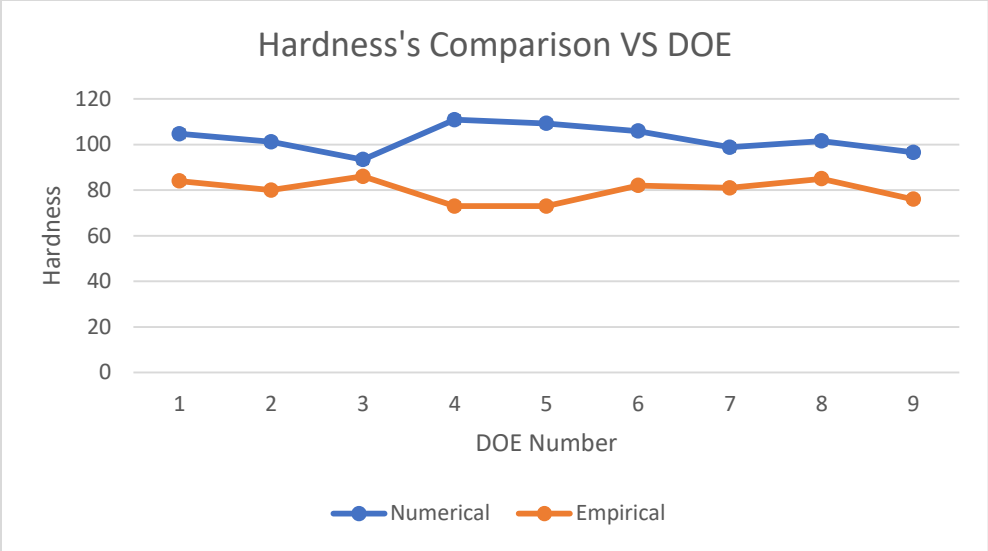

Fig. 23 Hardness's comparison obtained from both experiments and simulations

4. Conclusions

In this work, brass 405-20 was friction stir welded using two weld factors namely rotational speed and traverse speed. Full factorial design of experiments (DOEs) was implemented for both numerical and empirical research works. Three response parameters were focused mainly including thermal distribution at HAZ, joint strength, and hardness at the HAZ. Two numerical FEA studies were performed including transient thermal analysis (FEA_A) and static structural analysis (FEA_B). Thermal outputs of FEA_A were inputted to the FEA_B to find the stress at joint and joint hardness. Following were the main findings during current numerical and empirical investigational settings:

- Numerical studies performed were found in good agreement with the empirical work except few discrepancies for joint hardnesses.
- Optimal FSW factors' levels were found to be 1450 rpm and 60 mm/min for DOE4 in full factorial settings.
- Maximum temperature was found to be 598 ^{o}C which was well below the melting point of brass. So, successful friction stir welding of brass was validated in terms of its basic definition of solid-state welding. This temperature was found for DOE4.
- Maximum joint strength was found to be 212 MPa at DOE4 which is 77.1% of base brass.
- Hardness was found to be the lowest for DOE4 i.e. 73 HR validating further that DOE4 is an optimal combination of both rotational speed and traverse speed.

Acknowledgements

This work is based on the research initiatives for friction stir welding of brass by the first author i.e. Syed Farhan Raza. Moreover, the authors are really indebted to the University of Engineering and Technology, Lahore, Pakistan for the research facilities used in this research.

Authors' contribution

Syed Farhan Raza: Conceptualization, Data analysis, Resources, Methodology, Writing-original draft, Sarmad Ali Khan: Methodology, Data analysis, Writing, Investigation, Muhammad Farhan: Methodology, Data analysis, Writing, Investigation, Naveed Ahmed: Review & editing, Muhammad Salman Habib: Resources, Review and editing, Data analysis and curation, Ahmed M. Mehdi: Data curation, Review & editing.

Funding

The current research work does not have any funding to accomplish current research.

Data availability

The data related to experimental findings is already reported within the paper, and it can also be available from corresponding author 'Ahmed M. Mehdi' upon a reasonable request.

Declarations

Competing interests

The authors state that they have no conflict of interest or personal relationships that could have appeared to influence this work.

Ethics approval and consent to participate

The authors confirm that they have abided by the publication ethics, state that this work is original, and have not been used for publication anywhere before.

Consent for publication

The authors give consent to the journal regarding the publication of this work

References

[1] X. He, F. Gu, and A. Ball, "A review of numerical analysis of friction stir welding," *Prog. Mater. Sci.*, vol. 65, pp. 1–66, 2014, doi: 10.1016/j.pmatsci.2014.03.003.

[2] J. Overview and A. Laska, “Properties of Butt Friction Stir Welded,” pp. 1–46, 2020.

[3] D. M. Neto and P. Neto, “Numerical modeling of friction stir welding process: A literature review,” *Int. J. Adv. Manuf. Technol.*, vol. 65, no. 1–4, pp. 115–126, 2013, doi: 10.1007/s00170-012-4154-8.

[4] M. Song and R. Kovacevic, “Heat transfer modelling for both workpiece and tool in the friction stir welding process: A coupled model,” *Proc. Inst. Mech. Eng. Part B J. Eng. Manuf.*, vol. 218, no. 1, pp. 17–33, 2004, doi: 10.1243/095440504772830174.

[5] P. Biswas and N. R. Mandal, “Effect of tool geometries on thermal history of FSW of AA1100,” *Weld. J.*, vol. 90, no. 7, 2011.

[6] H. Zhang, J. H. Huang, S. B. Lin, L. Wu, and J. G. Zhang, “Temperature simulation of the preheating period in friction stir welding based on the finite element method,” *Proc. Inst. Mech. Eng. Part B J. Eng. Manuf.*, vol. 220, no. 7, pp. 1097–1106, 2006, doi: 10.1243/09544054JEM425.

[7] D. K. Yaduwanshi, S. Bag, and S. Pal, “Heat transfer analyses in friction stir welding of aluminium alloy,” *Proc. Inst. Mech. Eng. Part B J. Eng. Manuf.*, vol. 229, no. 10, pp. 1722–1733, 2015, doi: 10.1177/0954405414539297.

[8] A. R. S. Essa, M. M. Z. Ahmed, A. K. Y. A. Mohamed, and A. E. El-Nikhaily, “An analytical model of heat generation for eccentric cylindrical pin in friction stir welding,” *J. Mater. Res. Technol.*, vol. 5, no. 3, pp. 234–240, 2016, doi: 10.1016/j.jmrt.2015.11.009.

[9] S. Memon, A. Murillo-Marrodán, H. M. Lankarani, and H. Aghajani Derazkola, “Analysis of friction stir welding tool offset on the bonding and properties of al–mg–si alloy t-joints,” *Materials (Basel).*, vol. 14, no. 13, pp. 1–18, 2021, doi: 10.3390/ma14133604.

[10] M. B. Durdanović, M. M. Mijajlović, D. S. Milčić, and D. S. Stamenković, “Heat generation during friction stir welding process,” *Tribol. Ind.*, vol. 31, no. 1–2, pp. 8–14, 2009.

[11] C. Meran, “The joint properties of brass plates by friction stir welding,” *Mater. Des.*, vol. 27, no. 9, pp. 719–726, 2006, doi: 10.1016/j.matdes.2005.05.006.

[12] F. Hugger, K. Hofmann, S. Stein, and M. Schmidt, “Laser beam welding of brass,” *Phys. Procedia*, vol. 56, no. C, pp. 576–581, 2014, doi: 10.1016/j.phpro.2014.08.045.

[13] G. Çam, H. T. Serindağ, A. Çakan, S. Mistikoglu, and H. Yavuz, “The effect of weld parameters on friction stir welding of brass plates,” *Materwiss. Werksttech.*, vol. 39, no. 6, pp. 394–399, 2008, doi: 10.1002/mawe.200800314.

[14] H. S. Park, T. Kimura, T. Murakami, Y. Nagano, K. Nakata, and M. Ushio, “Microstructures and mechanical properties of friction stir welds of 60% Cu-40% Zn copper alloy,” *Mater. Sci. Eng. A*, vol. 371, no. 1–2, pp. 160–169, 2004, doi: 10.1016/j.msea.2003.11.030.

[15] A. Heidarzadeh, R. V. Barenji, V. Khalili, and G. Güleryüz, “Optimizing the friction stir welding of the α/β brass plates to obtain the highest strength and elongation,” *Vacuum*, vol. 159, no. August 2018, pp. 152–160, 2019, doi: 10.1016/j.vacuum.2018.10.036.

[16] H. R. S. and P. A. Colegrove, “Process Modelling, Chapter 10 in Friction Stir Welding and Processing,” in *Friction Stir Welding and Processing*, ASM International, 2007, pp. 187–217.

[17] K. S. Suresh, M. R. Rani, K. Prakasan, and R. Rudramoorthy, “Modeling of temperature distribution in ultrasonic welding of thermoplastics for various joint designs,” vol. 186, pp. 138–146, 2007, doi: 10.1016/j.jmatprotec.2006.12.028.

[18] V. Patel, W. Li, G. Wang, F. Wang, A. Vairis, and P. Niu, “Friction stir welding of dissimilar aluminum alloy combinations: State-of-the-art,” *Metals (Basel).*, vol. 9, no. 3, 2019, doi: 10.3390/met9030270.

[19] P. Zhang, S. X. Li, and Z. F. Zhang, “General relationship between strength and hardness,” *Mater. Sci. Eng. A*, vol. 529, no. 1, pp. 62–73, 2011, doi: 10.1016/j.msea.2011.08.061.